SUPERSONIC NOZZLE

Module 3A3 Full Technical Report

Aalok Patwardhan
Emmanuel College

Abstract

Two experiments were performed and their results compared. The validity of one-dimensional, adiabatic, inviscid flow theory was investigated by measuring the pressure distribution throughout a convergent-divergent nozzle set-up, and a normal shock-wave was observed in a larger supersonic wind tunnel using Schlieren photography. It was seen that the boundary layer growth affected the effective flow cross-sectional area and the theoretical assumptions were shown not to hold due to the shock-wave interaction with the boundary layer. The effects of viscosity were much greater for the convergent-divergent nozzle experiment where the Reynold's number was around 10^4.

1 Introduction

Convergent-Divergent nozzles are used for a variety of applications in fluid dynamics and the world of engineering. With these nozzles, fluids can be accelerated to velocities greater than Mach 1. This is useful for testing supersonic flows in wind tunnels, however the nozzles can also be found in applications such as rocket engines.
This experiment consisted of two parts:

- The development of flow in a small convergent-divergent nozzle.
- Observing a normal shock-wave in a supersonic wind tunnel.

The aims were:

- Analyse the pressure distributions in a convergent-divergent nozzle;
- Observe the phenomenon of choked flow and understand how flow visualisation can be achieved through Schlieren photography;
- Observe fundamental flow changes through a normal shock-wave;
- Appreciate the limitations and validity of one-dimensional, adiabatic, inviscid theory.

2 Theory

2.1 Convergent-Divergent Nozzle Inlet conditions

The pressure change across the mercury manometers can be obtained by considering a force balance on the mercury in the manometer. One end of a manometer is exposed to the air, so the pressure at the tapping point can be given by equation 1, where h denotes the manometer reading, and h_{atm} denotes the level of mercury corresponding to atmospheric pressure.

$$P_{tap} = P_{atm} + \rho g(h - h_{atm}) \tag{1}$$

To calculate mass flow rate equations 2 and 3 are used. Bernoulli's equation can be used as the flow is considered to be incompressible and invsicid until the entrance of the orifice plate. The mass flow rate calculation includes the discharge coefficent C_d which is defined as the ratio of actual mass flow rate to the theoretical flow rate. The orifice itself creates viscous effects due to the fact that the flow is not able to follow the sharp angles produced by the orifice hole.

$$P_{orfice,gauge} = \frac{1}{2}\rho V^2 \tag{2}$$

$$\dot{m} = C_d \rho A V \tag{3}$$

The pressure at the orifice is assumed to be the same as that measured at the wall, because there is a recirculation zone. The streamlines are parallel here and also the velocity is small leading to a roughly constant pressure. The flow then mixes in the plenum chamber creating a homogenous flow at the nozzle inlet. The nozzle inlet pressure can be assumed to

be the same as that of the plenum chamber which is a fair assumption as the plenum flow velocity is low.

2.2 Nozzle Flow

The flow in the nozzle is assumed to be isentropic, and this is true in the absence of shock-waves. It is possible to relate Mach number, cross sectional area and free stream velocity with equation 4. This shows that for supersonic flow a fractional increase in area will accelerate the flow and a deceleration will occur in subsonic flow. Also when there is no change in area for example in the throat of a nozzle or in the wrking section of a wind tunnel there will be no change in velocity.

$$\frac{dA}{A} = (M^2 - 1)\frac{dV}{V} \tag{4}$$

The maximum mass flow rate can be achieved at a Mach number of 1 ie. when the flow is sonic. This is referred to as the flow becoming choked, and no changes in pressure downstream of the choking location can propogate back upstream. The result of this is that a shock-wave is formed in the divergence if the pressure at the nozzle exit is reduced further.

Using the convervation of mass continutity, momentum and energy it is possible to derive a relationship between the Mach numbers of the flow upstream and downstream of the shock. This is given in the *CUED Tables* [1] as equation 5. It is to be noted that this holds true for a frame of reference in which the shock-wave has been brought to rest, and that the cross-sectional area is constant (this is true for shock-waves normal to the flow direction). However in our experiment this analysis can be carried out as the geometry of the divergence ensures the angle between the flow and the shock is not far from being perpendicular.

$$M_s = \left(\frac{1 + \frac{\gamma - 1}{2} M^2}{\gamma M^2 - \frac{\gamma - 1}{2}} \right)^{\frac{1}{2}} \tag{5}$$

A similar relationship can be found between stagnation pressure upstream and downstream of the shock-wave. This is useful as it is a measure of the strength of the shock-wave - how much entropy has been generated. The location of the shock-wave moves further downstream as back pressure is decreased, until it exits the nozzle completely and supersonic flow is present throughout the diveregent section of the nozzle. The same analysis holds true for the working section of a wind tunnel.

3 Experimental Method

3.1 Part 1 - Convergent-Divergent Nozzle

The experimental apparatus consisted of a small open-circuit convergent-divergent nozzle, connected to a plenum chamber on the upstream end. Air was taken in from the atmosphere and passed through an orifice plate into a plenum chamber before entering the nozzle. The air was drawn in by a compressor and the back pressure (downstream of the nozzle) could be controlled by opening a control valve. The function of the plenum chamber was to ensure a constant inlet pressure, and the orifice plate enabled measurement of the flow rate. Pressure tappings were located along the nozzle and connected to mercury manometers to measure variation in pressure.

The orifice plate pressure drop, which was much lower than the pessure drop along the nozzle, was measured by a water manometer. Using water, which has a much lower density than mercury, ensured that the accuracy of measurement was high.

However the majority of errors stem from the orifice plate presure drop which leads to erros in the calculated mass flow and in cross-sectional area. Turbulence led to fluctuating readings which decrease the accuracy in measuring pressure and Mach number.

Using the control valve to vary back pressure, four runs were conducted to analyse the different flow cases:

1. Subsonic flow throughout the nozzle.
2. Choked flow (sonic) at the nozzle throat, but subsonic in divergence.
3. Supersonic flow in the divergence creating a shock-wave there.
4. Supersonic flow throughout the nozzle divergence.

3.2 Part 2 - Supersonic Wind Tunnel

A convergent-divergent nozzle in a wind tunnel with a larger cross sectional area was used to create uniform supersonic flow in the working section. Apart from a circular Pitot tube and needle shaped static pressure probe the working section was empty.
Optical techniques such as Schlieren photography and shadowgraph imaging were used to visualise the flow as a shock-wave propagated through the working section.

In shadowgraph imaging, light from a point source located at the focal point of a convex mirror is reflected by the mirror as parallel rays which travel through the wind tunnel working section. The rays are then collected on the other side of the tunnel by another convex mirror and focused onto the recording equipment (in this case a camera lens). Light is refracted by changes in the flow density and so the image received by the camera contains a higher intensity of light corresponding to the region where there has been an increase in density. Across a shock-wave there is a sudden increase in density so we can use Shadowgraph imaging to visualise the wave.

Schlieren photography operates under the same principles as shadowgraph imaging, with the addition of a knife edge which is placed at the focal point of the second mirror (before the camera). This removes completely any light which was diffracted, resulting in a much higher contrast in the final image.

It can also be noted that the Schlieren method measures the first derivative of density, whilst the Shadowgraph method measures the second derivative. Figure 1 shows the schematic layout of the shadowgraph/Schlieren set up used in the experiment.

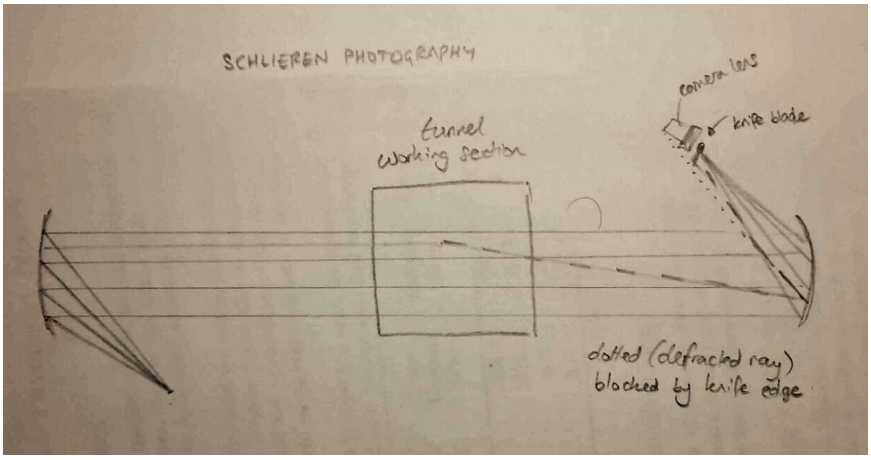

Figure 1

4 Results and Discussion

4.1 Part 1 - Convergent-Divergent Nozzle

4.1.1 Shock Strength

The pressure plots for all four runs are given in figure 3 in the Appendix. For run 3 there is an increase in pressure ratio around tapping points 15-17. Although a sudden jump in ratio is to be expected here the results show that a gradual increase is seen in reality. This is due to the interaction of the shock-wave and the boundary layer generated along the nozzle wall. Figure 4 in the Appendix shows this interaction. Flow cannot be considered under the inviscid assumption here and so the pressure readings which are taken along the wall are smeared or distorted.

A reasonable approximation as suggested in the handout is to assumer the shock-wave location has the same pressure ratio as that at the throat where M = 1. This implies that the location of the shock was at pressure tapping 16.
A fully inviscid flow as in run 4 of the experiment can give the pressure ratio just before the shock location. The Mach number of the flow at tapping 16 for run 4 was found to be 1.37, and the CUED Compressible Flow Data Book [1] gave a value of $M_s = 0.75$.

4.1.2 Throat Area and Nozzle Exit Area

Using equations 2 and 3 the mass flow rate for each run is calculated, and the cross sectional area of the nozzle throat can be calculated by using the non-dimensionalised mass flow at M=1 from the Data Book [1] written in terms of throat area A^*:

$$A^* = \frac{\dot{m}\sqrt{c_p T_0}}{1.281 * P_0}$$

The mass flow rates for runs 2-4 were calcluated and are shown in table 1 and an average mass flow rate of 0.00523 kgs^{-1} was obtained.

	Gague Pressure (Pa)	Velocity (m/s)	Mass Flow x Cd (kg/s)
Run 1	353.2	24.01	4.37E-03
Run 2	510.1	28.86	5.25E-03
Run 3	500.3	28.58	5.20E-03
Run 4	510.1	28.86	5.25E-03

Table 1

The cross sectional area of the throat was thus calculated to be $A^*=21.7mm^2$, compared to the actual value given in the handout of $A=22.6mm^2$. This error of 3.98% can be attributed to the fact that there is a boundary layer present which reduces the free stream flow area.

Using the flow Mach numbers at the nozzle exits, the cross-sectional area for each run was calculated. For run 3, the analysis was not as simple. As the shock was assumed to occur at tapping 16, the Mach number for run 4 at tapping 16 was taken (M=1.37), giving a post-shock Mach number of M=0.75, with a ratio of stagnation pressure (post-shock to pre-shock) to be $P_{0S}/P_0 = 0.965$. From this, the nozzle exit area was calculated and the results are tabulated in table 2.

	Mass flow (kg/s)	Mach number at nozzle exit	Non-Dimensional Mass flow	Nozzle exit area (mm^2)
Run 1	0.004372	0.56	1.033	22.49
Run 2	0.005254	0.69	1.163	24.01
Run 3	0.005203	0.75	1.206	23.75
Run 4	0.005254	1.43	1.132	24.67

Table 2

The different results for the nozzle exit area can be accounted for partly due to the uncertainties in calculating exit Mach numbers, however a more prominent reason is due to the presence of friction in the divergent section of the nozzle generating a thickening boundary layer.

Some of the pressure distributions display a 'bulge', and this could be linked to the boundary layer. The bulge is where the pressure ratio has seemingly become flat or slightly increasing; this is perhaps most prominent for runs 3 and 4. If the boundary layer thickness is increasing at a similar rate to the cross-section diameter, then the effective free stream flow area is roughly constant and this would keep the pressure ratios constant. This increased rate of boundary layer growth could be due to its transitioning to a turbulent regime.[3] This is shown in figure 2. More experiments are required to evaluate the flow regimes in this nozzle.

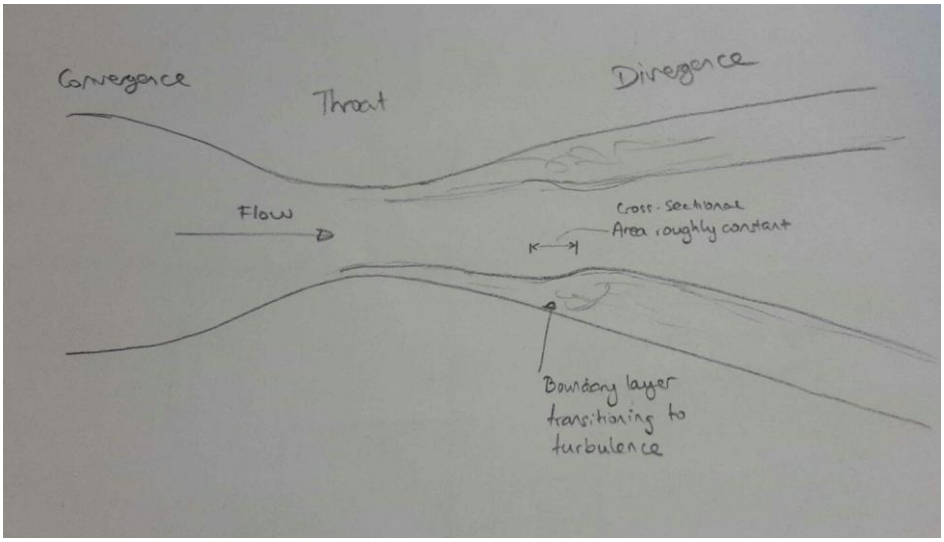

Figure 2

4.2 Part 2 - Supersonic Wind Tunnel

4.2.1 Stagnation Pressure Ratio Across Shock-wave

It can be seen from the pressure plots of stagnation pressure in figure 5 in the Appendix that the values did not depend on the location of the shock-wave. This is because a Pitot tube works by stagnating the flow, which must mean the supersonic flow becomes subsonic in front of the tube, resulting in a bow shock-wave being always present in front of the Pitot tube. From the design value of the Mach number for the wind tunnel to be M=1.5, the expected ratio of stagnation pressures P_{0S}/P_0 was 0.930, however the ratio from the experiment was $P_{0S}/P_0 = 0.937$ corresponding to M = 1.475.

4.2.2 Static Pressure Ratio Across Shock-wave

The ratio of static to stagnation pressure upstream of the shock $P/P_0 = 0.285$ corresponds to M = 1.470, which is consistent with the above analysis. However comparing the theoretical and measured ratios of static to upstream stagnation pressure yields differring results. From the results, $P_S/P_0 = 0.609$, however the theoretical ratio (using M=1.75) gives P_S/P_0 = 2.370*0.282=0.668, a much higher value. Downstream of the shock-wave the boundary layer thickness increases and reduces the cross sectional area of the free streem. As a result the Mach number increases and leads to a lower pressure ratio.

4.3 Comparison of the two experiments

It is clear to see that the interaction between the boundary layer and shock-waves are one of the primary reasons for results deviating from theoretical analysis. The shock-wave is smeared closer to the boundary layer and is not normal to the flow direction. This causes the pressure change across the shock to be not as sudden as theory suggests. The separation of the boundary layer due to the adverse pressure gradient at the shock invalidates the one dimensional flow assumption.

Although viscous effects affect both experiments, the results indicate that the convergent-divergent nozzle suffers the worst. The Reynold's number for the first experiment was around 10^4 whereas for the wind tunnel the Reynold's number was around $3x10^5$. This meant that viscous effects were much more dominant was the first experiment than for the second. Comparing the sizes of the flow cross-sectional area, the nozzle from this first experiment has a cross-sectional area around 1000 times smaller than that of the large wind tunnel. The ratio of boundary layer thickness to cross-sectional diameter is much greater for the first experiment than for the wind tunnel experiment and this causes stronger deviations from theory.

5 Conclusion

Comparing the two experiments, conclusions can be drawn about the validity of one-dimensional theory in nozzle flows. In particular, a shock-wave can cause a considerable increase in boundary layer thickness due to the large adverse pressure gradient across it and thus the flow must not be considered one-dimensional. The boundary layer also smears the shock-wave near the walls meaning the normal shock assumption is not correct here and the pressure change across the shock is gradual instead of sudden.

It was also seen that pitot tubes are insensitive to shock location as they only measure stagnation pressure downstream of the shock.

Finally the effects of viscosity cannot be neglected if a shock-wave is present. The convergent-divergent nozzle experiment is affected the most by these effects due to the relative size of the boundary layer in the nozzle being larger than that in the wind tunnel experiment.

References

[1] CAMBRIDGE UNIVERSITY. *CUED Compressible Flow Data Book, 2009.*
[2] J ANDERSON. *Modern Compressible Flow.* MCGRAW-HILL, third edition, 2003.
[3] K. C. SAHU and R. GOVINDARAJAN. *J. Fluid Mech. Stability of flow through a slowly diverging pipe, vol 531.* CAMBRIDGE UNIVERSITY PRESS, 2005.

Appendix

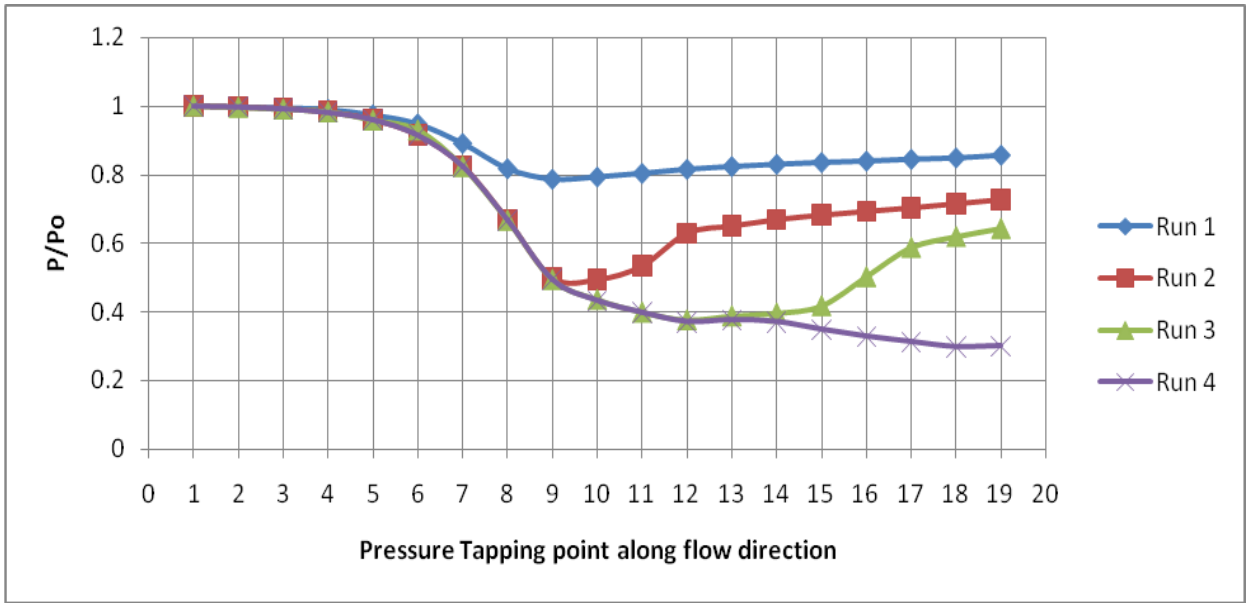

Figure 3

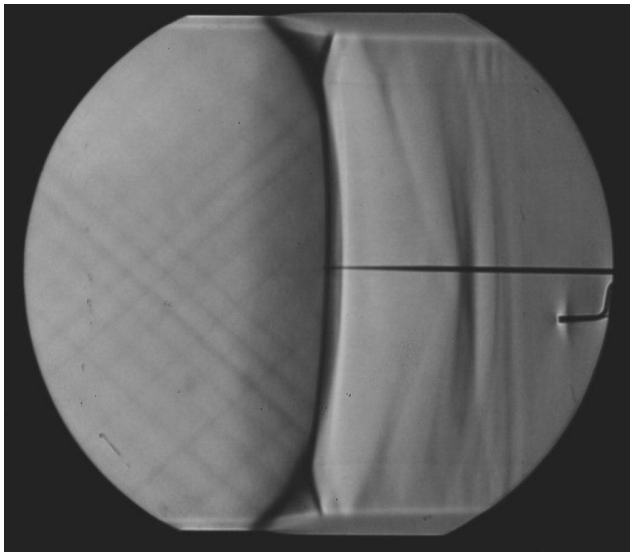

Figure 4

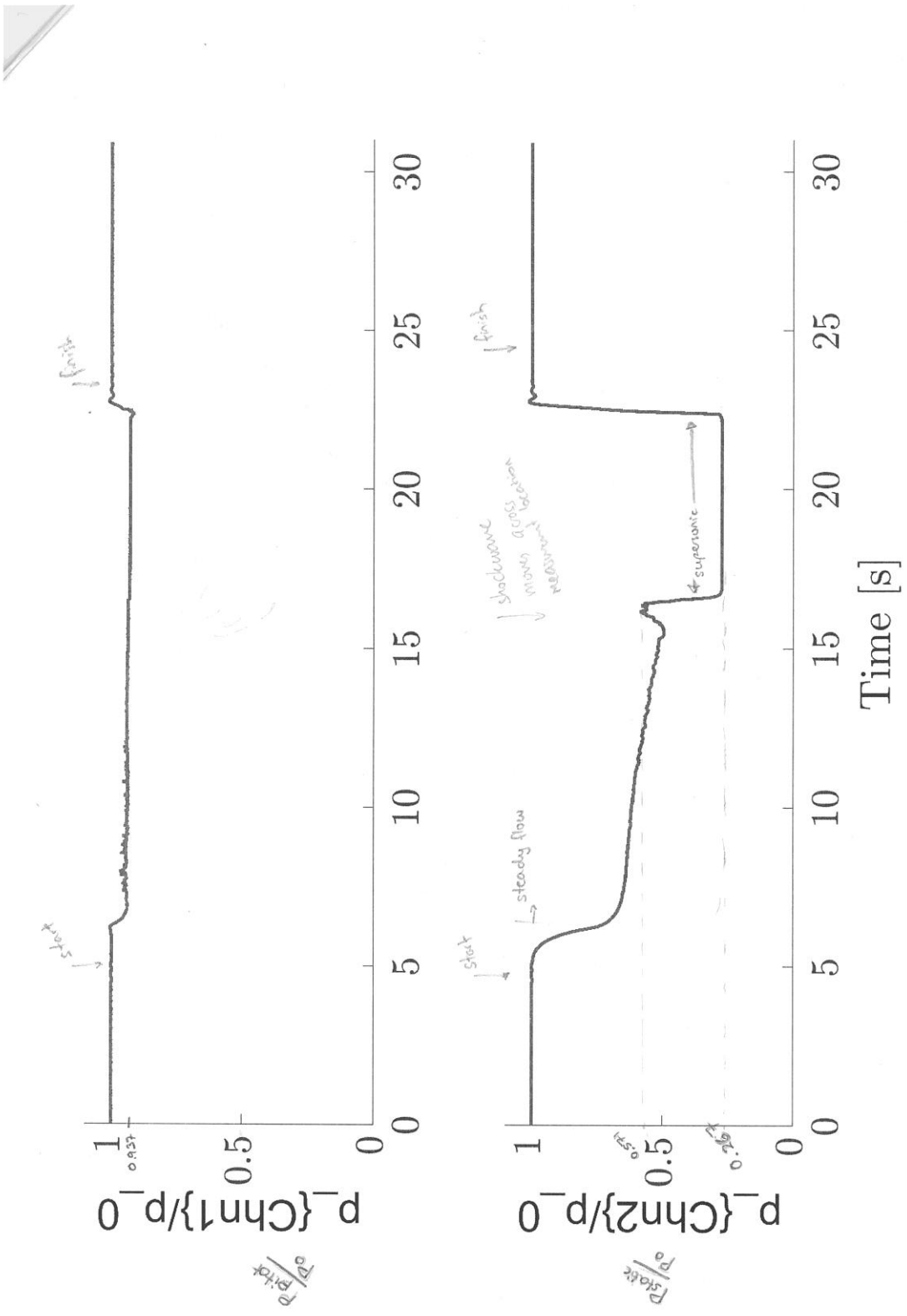
p_{Chn1}/p_0
p/p_tot
start
finish
0.937
p_{Chn2}/p_0
p_static/p_0
start
steady flow
shockwave
finish
supersonic
0.527
0.245
Time [s]
0
5
10
15
20
25
30
0.5
1

Figure 5